Journal of Power Sources 240 (2013) 458–470

Contents lists available at SciVerse ScienceDirect

Journal of Power Sources

journal homepage: www.elsevier.com/locate/jpowsour

Structural and thermal properties of glass composite seals and their chemical compatibility with Crofer 22APU for solid oxide fuel cells applications

Gurbinder Kaur [a,*], K. Singh [b], O.P. Pandey [b], D. Homa [a], B. Scott [a], G. Pickrell [a]

[a] Department of Material Science and Engineering, Holden Hall, Virginia Tech, Blacksburg, VA 24060, USA
[b] School of Physics and Materials Science, Thapar University, Patiala 147004, India

HIGHLIGHTS

- Glass composite seals are prepared by ball-milling different glasses in fixed ratio for 5 h.
- No reactive particle was used in glass matrix to obtain composites.
- The structural characteristics of composites were studied using XRD, particle size and zeta potential.
- The chemical compatibility of these composites was investigated with Crofer 22APU.
- The interface and resulting microstructure was morphologically characterized by using SEM/EPMA.

ARTICLE INFO

Article history:
Received 11 January 2013
Received in revised form
28 February 2013
Accepted 25 March 2013
Available online 3 April 2013

Keywords:
Glass composite
Solid oxide fuel cell (SOFC)
Scanning electron microscopy (SEM)
Chemical interaction
X-ray diffraction (XRD)
Diffusion

ABSTRACT

In the present investigation, glass composite seals have been prepared by mixing the different glass compositions in fixed ratio and then ball milling for 5 h. The main aim of this approach is to investigate the sealing and bonding issues in solid oxide fuel cells (SOFC) without using unreactive particles in glass matrix. The structural and thermal characteristics of these composites were studied using particle size analyzer, zeta potential, dilatometry, differential scanning calorimetry (DSC) and thermogravimetric analysis (TGA). X-ray diffraction has revealed phase formation in all composites after 1000 h heat-treatment at 850 °C. In addition to this, the chemical compatibility of the prepared glass composites with the interconnect Crofer 22APU has been studied using scanning electron microscope (SEM), electron probe microanalysis (EPMA), energy dispersive spectroscopy (EDS) and dot-mapping techniques. The interfacial study has revealed that GG6 and GG7 composites have good adhesion without delamination, cracks or pore formation. Chromate formation occurred in GG3 and GG4 composite couples, though no delamination was observed at the interface of GG4 composite with Crofer 22APU. GG5 could not form a diffusion couple due to its high viscosity and very low coefficient of thermal expansion.

1. Introduction

High temperature solid oxide fuel cells (SOFC) can generate power from a variety of fuels. Their solid geometry, high efficiency along with environment friendly byproducts has lead to a broad range of applications like aeronautics, power generation in automobiles and various electronic devices [1–5]. Usually planar and tubular geometries are the most preferred designs for SOFC operation. The short current path for planar SOFC results in a high power density as compared to the tubular design [6–8]. However, hermetic seals are required for planar SOFC to bond cell components together, prevent leakage losses and direct combustion of fuel and oxygen. In addition to this, these hermetic seals should fulfill many stringent requirements in order to be a suitable sealing material for SOFC operation [9–13]. The most important requirement is mechanical and chemical compatibility of seals with adjoining components in reducing/oxidizing atmospheres at high temperatures between 600 and 1000 °C for prolonged periods of operation.

The general approaches for sealing include compressive, compliant, rigid bonded and composite [14–16]. Compliant seals do not bond well to SOFC components resulting in hydrogen embrittlement whereas compressive seals require load. Rigid bonded seals like glass and glass ceramics are preferred seals due to their

* Corresponding author. Tel.: +1 540 239 7929.
E-mail address: gkaur82@vt.edu (G. Kaur).

0378-7753/$ – see front matter © 2013 Elsevier B.V. All rights reserved.
http://dx.doi.org/10.1016/j.jpowsour.2013.03.142

endurance in stringent operating conditions. In addition to this, their properties can be tailored by carefully choosing the proper initial composition [17–22]. But generally, these glasses are prone to cracking. In order to increase the mechanical endurance of glass seals, they are reinforced with unreactive particles to form a composite [23–26]. The flexure strength as well as fracture toughness is higher for composites [26]. Magnesia particles have been suspended in sodium aluminosilicate glass matrix by Nielsen et al. [27]. These composites exhibited excellent wetting characteristics with the interconnect material. Smeacetto et al. [25] used alumina to increase the seal viscosity, thermal shock resistance and coefficient of thermal expansion (CTE). Composites can improve thermo-mechanical properties of the composite seal. The particle size and volume fraction of the second phase helps control the properties of the composite. The glass matrix can convert to a more stable crystallized phase, which subsequently flows to mitigate the stresses [28–30].

In the present investigation, a new approach to make glass composites has been studied. Instead of incorporating the unreactive particles in a glass matrix, the glasses have been mixed in fixed ratio and then ball-milled for 5 h. The idea behind this new approach is to develop a novel seal, which could address the chromate formation, and sealing capability along with improved viscosity as well as CTE without dispersing filler material (unreactive) in glass matrix. At high temperatures, these filler materials can easily segregate and hence increase the stress within sealing materials further leading to cracks and loss of structural integrity. On the other hand, the composite of two glassy materials is chemically more compatible to each other, which can reduce the thermal stress at working temperature of SOFCs. Moreover, a uniform and homogenized glass composite could be obtained by high energy ball milling, which could further help in improving particle size, viscosity and adhesion behavior. The glass compositions used to make composites have been chosen from our previous investigations [31–36]. The physical and thermal characteristics of these composites were studied using particle size analyzer, zeta potential, differential scanning calorimetry (DSC) and thermogravimetric analysis (TGA). Using dilatometric analysis, the coefficient of thermal expansion and viscosity of all these composites have been calculated. The various phases formed for composites after heat-treatment at 850 °C for 1000 h were studied using X-ray diffraction (XRD). Furthermore, the chemical compatibility of prepared glass composites with interconnect Crofer 22APU for 1000 h at 850 °C has been studied using scanning electron microscope (SEM), electron probe microanalysis (EPMA), energy dispersive spectroscopy (EDS) and dot-mapping techniques. The main aim of this approach is to investigate the sealing and bonding issues in SOFC.

2. Experimental techniques

The preparation details of the ML, CL, SL and BL glasses chosen for the present study are given elsewhere [31,32]. These glass compositions are mixed in ratio 1:1 and then ball-milled for 5 h. The composition with sample labels is shown in Table 1. The particle size, zeta potential and conductivity at room temperature of the prepared samples were determined using dynamic light scattering based Zetasizer nano series. The sample of concentration 0.1 g l^{-1} was prepared using methanol as a reference solution. The density of glass composites was calculated using Archimedes principle. The glass transition temperature (T_g) and crystallization temperature (T_c) was obtained using differential scanning calorimetry (DSC). The DSC and weight loss measurements were carried out in Netzsch 402 EP using alumina as the reference material and in an air atmosphere. The DSC measurements of all the composites were done at different heating rates (10, 20, 30, 40 °C min^{-1}) to calculate the activation energy for crystallization (E_c). The dilatometer study was performed using Netzsch DIL 801 L in the temperature range of 100-softening temperature (T_s) to determine the coefficient of thermal expansion (CTE) of 1000 h heat-treated as well as pristine glass composite and also to study the effect of crystalline phase formation on CTE.

The crystalline phases formed in the 1000 h heat-treated glass composites were analyzed using high-resolution XRD in an X'Pert PRO diffractometer (PANalytical B.V., EA Almelo, The Netherlands). The XRD voltage was 45 kV and the beam current was 40 mA. The scan time per step was 300 s with CuK_α radiation (λ = 1.5406 Å). The phase identification was done by comparing the experimental diffractograms to standard patterns complied by the International Centre for Diffraction Data (ICDD).

For interaction study, Crofer 22APU/glass composite diffusion couples were prepared using a slurry technique. The Crofer 22APU (Thyssenkrupp VDM GmbH) pieces were cut into 9 mm × 8 mm × 3 mm dimensions. These pieces were ultrasonically cleaned in acetone. The glass composite powder was dispersed in ethanol and then deposited between Crofer 22APU plates to make sandwich like structure. The joining thermal treatment to the couples was performed in tubular furnace at temperature above glass softening temperature (from 0 to 900 °C). The heating rate was kept at 30 °C min^{-1} and a dwell time of 45 min was used at 900 °C. The diffusion couples were heat-treated at 850 °C in tubular furnace for 1000 h. Diffusion couples were polished mechanically and etched with dilute HF. These polished and etched diffusion couples were analyzed under environmental ESEM (FEI Quanta 600 FEG, Hilsboro) with ET detector and 4000 Pa pressure. The elemental analysis was done Bruker QUANTAX 400 Energy Dispersive X-ray Spectrometer (high speed Silicon Drifted Detector) in order to study the interaction and diffusion of ions.

3. Results and discussion

3.1. Particle size, density and zeta potential

The particle size, zeta potential and density obtained for all the composites are listed in Table 1. The average particle size of ML, CL, SL and BL glass is 3.07, 3.56, 5.48 and 6.92 μm respectively. The average particle size and zeta potential for sample GG1 are shown in Fig. 1(a) and (b) respectively. The GG3 sample has the highest

Table 1
Composition of glass composites along with particle size, zeta potential, conductivity at room temperature and density.

Sample name	Composition (1:1)	Particle size d (μm)	Zeta potential (mV)	Conductivity at room temperature ($\times 10^{-11}$ S cm^{-1})	Density (gm cc^{-1})
GG1	ML + CL	1.52	10.11	6.42	3.42
GG2	CL + SL	3.22	22.51	1.66	3.68
GG3	SL + BL	6.05	51.18	3.13	4.01
GG4	BL + ML	3.93	26.42	4.16	3.82
GG5	BL + CL	5.12	36.82	1.48	3.91
GG6	ML + SL	5.17	38.93	2.87	3.54
GG7	ML + CL + SL + BL	5.54	48.92	2.02	3.85

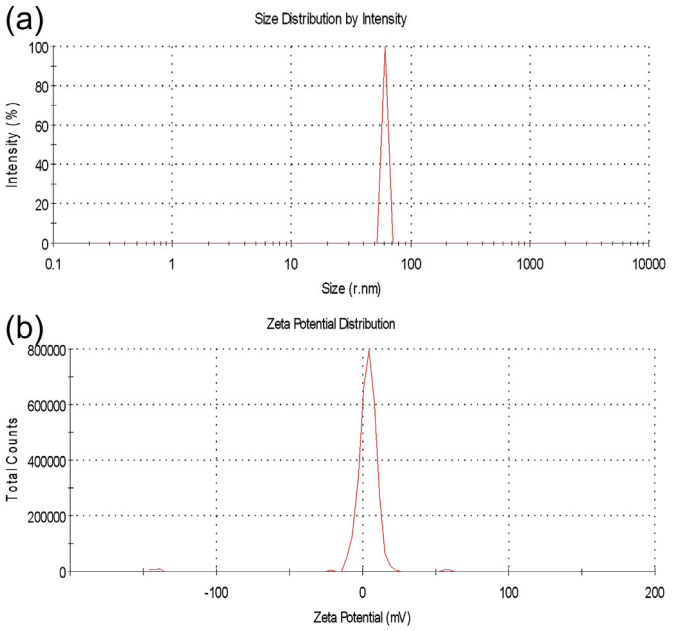

Fig. 1. (a) Particle size distribution and (b) zeta potential for GG1 composite.

particle size, whereas the GG1 composite has the smallest size. This may be due to the fact that G1 contains small cations like Ca^{2+} and Mg^{2+} whereas GG3 has big Sr^{2+} and Ba^{2+} cations. At the same time, the zeta potential is also highest for the GG3 sample and lowest for GG1 sample. Zeta potential generally gives the flocculation tendency of particles. If particles have low zeta potential, then no force can prevent them from coming together. The repulsion between particles of higher zeta potential precludes the possibility of flocculation. In other words, zeta potential gives a direct measure of inter-particle repulsive force [37,38]. For high strength and stable particles, high zeta potential is required. The GG1 glass composite has minimum zeta potential. Again small cations associated with GG1 composite could lead to its small zeta potential. The particle size and zeta potential have followed the same trend in the present investigation, which implies that the composite with highest particle size has high zeta potential. The stability of the composites could follow the order GG3 > GG6 > GG2 > GG7 > GG5 > GG3 > GG1. The density of all the samples lies between 3.42 and 4.01 gm cc^{-1}. The high density of the GG3 sample indicates its high cross-linking density in its network. The conductivity obtained at room temperature has been listed in Table 1. All the composites have conductivity of the order of 10^{12} S cm^{-1}. Sample GG1 exhibits maximum conductivity indicating the small ionic size of cations could lead to ease of ionic motion.

3.2. X-ray diffraction (XRD) analysis

The XRD of all the glass composites heat-treated at 850 °C for 1000 h is shown in Fig. 2. The GG1 glass has shown the formation of $CaMgSi_2O_6$ (ICDD-831817) phase with $La_{9.33}Si_6O_{26}$ (ICDD-490443) as a minor phase. For the GG2 glass composite, the $Ca_{1.8}Sr_{0.2}SiO_4$ (ICDD-771621) phase was formed without any other phase. Two phases precipitated out for the GG3 composite i.e. $BaSrSi_3O_8$ (ICDD-280158) and $BaSiO_3$ (ICDD-702112). For GG4 composite, $Ba_2MgSi_2O_7$ (ICDD-860419) and $La_{9.31}$ $(Si_{1.04}O_4)_6$ O_2 (ICDD-752956) phases have been obtained after a 1000 h treatment. The major phase for GG5 glass is $CaSiO_3$ (ICDD-840655) whereas the minor phase is $Ba_{1.3}Ca_{0.7}SiO_4$ (ICDD-480210). The GG6 composite has Sr_2SiO_4 (ICDD-100034) and $La_2Si_2O_7$ (ICDD-722456) phases. For the GG7 composite, Ba_2SiO_4 (ICDD-770150) and $Ca_{0.75}$ $Sr_{0.2}Mg_{1.05}Si_2O_6$ (ICDD-800388) have precipitated. The calcium, magnesium and strontium have formed a solid solution phase, whereas barium has formed a separate silicate phase.

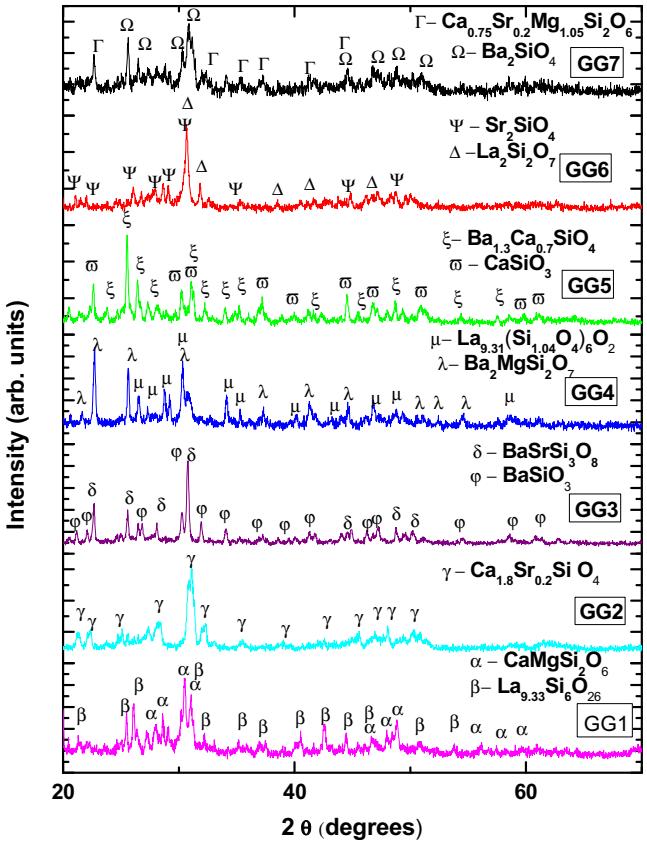

Fig. 2. XRD of all glass composites after 1000 h heat-treatment at 850 °C.

Alkaline earth atoms and lanthanum have higher tendency to bond with glass forming cations via non-bridging oxygen atoms [39,40]. La–Si–O units also act as nucleation sites inside the network [41]. The GG1, GG4 and GG6 samples have shown the formation of lanthanum silicate phases whereas the GG2, GG3, GG5 and GG7 composites have shown only alkaline silicate phase formation. Interestingly, magnesium-containing glasses except GG7 have shown the presence of lanthanum silicate phases indicating La–Si–O units to be the predominant nucleation sites in these composites. Furthermore, no magnesium silicate phases have been observed for these composites. The field strength of Mg^{2+}, Ca^{2+}, Sr^{2+} and Ba^{2+} varies as 0.45, 0.33, 0.30 and 0.24 respectively [42]. Accordingly the activation energy of magnesium is expected to be high. Only the GG2 composite is single phase and all other composites are double phase. But even after a 1000 h heat-treatment, the crystallized fraction of GG2 is small and has a large amorphous glassy matrix as compared to other composites.

3.3. DTA/TGA

Non-isothermal method is widely used to obtain various characteristic parameters from DTA [43,44]. In this method, the sample is heated at a fixed heating rate. It is assumed that there is variation in peak crystallization temperature with increasing heating rate (β). The thermal stability of the glass composites was investigated using thermogravimetric analysis (TGA). The stability of the glass composite at higher temperature can easily be predicted by TGA by measuring weight loss. B_2O_3 is known to be volatile at higher

temperatures, The TGA can predict the degree of volatility in a particular composite accurately [45,46]. The glass transition temperature (T_g), glass crystallization temperature (T_c) and weight loss for all the composites is listed in Table 2. The data obtained from DTA was used to calculate the activation energy of crystallization. Activation energy is the threshold energy above which the transformation can take place in the activated complex. The activation energy at the peak of crystallization (E_c) is obtained using Augis and Benett model as follows [43]:

$$\ln(T_c/\beta) = E_c/RT_c + \ln\nu \quad (1)$$

where ν is defined as the number of attempt, which are made by the nuclei/second for overcoming the energy barrier. The Augis and Benett model gives idea about the nucleation sites in terms of frequency factor besides activation energies. The activation energies are also listed in Table 2.

The GG1 composite has minimum activation energy. The GG2 has the highest activation energy of crystallization followed by GG6. Moreover, the frequency factor for GG2 sample is 8.67×10^8, which signifies 8.67×10^8 attempts per second by nuclei to overcome the energy barrier. The value of frequency is smallest for the GG2 among all the composite samples indicating its higher devitrification resistance. This is in correlation with XRD of GG2 as it is showing only single phase whereas all other composites have double phase formation. The phase fraction in case of the GG6 is also small. Devitrification can be due to small nuclei formed during quenching of the melt, surface flaws and residual stresses arising from mechanical polishing [47–49]. Within certain region, the localized ordering can lead to heterogenous nucleation sites, which further help in triggering the devitrification process [49,50]. Lanthanum containing glasses generally possess clusters of La–O–La order phase units acting as nucleation sites [50,51]. Sample GG6 and GG7 have small weight loss indicating their structural stability. GG1 shows maximum weight loss and hence loose network. All other samples display acceptable range of weight loss.

3.4. Dilatometric analysis

The glass transition temperature (T_g), glass softening temperature (T_s) and coefficient of thermal expansion obtained from the dilatometric studies have been listed in Table 2. GG5 sample has lowest and GG3 possess highest CTE respectively. Generally stronger materials possess smaller changes in CTE [42]. All the compositions except GG5 display acceptable CTE i.e. $(9.30–10.89) \times 10^{-6}$ K^{-1} which is in good agreement with the interconnect. Various reports in literature indicate the difference of $(1–1.5) \times 10^{-6}$ K^{-1} among various components of SOFC to be acceptable [12,52]. High ionic radii of Ba^{2+} and Sr^{2+} may be responsible for high CTE of GG3. After 1000 h heat-treatment, GG5 glass has shown a decrease in CTE. The decrease in CTE of the GG5 glass could be attributed to the formation of a $CaSiO_3$ phase. $CaSiO_3$ is a low CTE phase whereas for GG5 the formation of barium silicate phase has taken place, which is generally associated with higher CTE [13]. Generally lanthanum based glasses possess higher CTE due to its higher ionic radii and lower field strength. Heat-treatment turns glass into glass ceramic. The formation of a crystalline phase may increase or decrease the CTE of the parent composition depending upon the nature of phase formed.

The dilatometer data has been used to calculate the viscosity. Viscosity is a measure of fluidity i.e. a melt with higher viscosity has a higher resistance to flow. Viscosity can also determine the conditions under which crystallization/devitrification occurs. The Vogel–Fulcher–Tamman (VFT) equation provides a good fit to viscosity data over the entire range [42]. The viscosity of composites have been determined using VFT eqn. as follows:

$$\log\eta = A + \frac{B}{T - T_o} \quad (2)$$

where A, B and T_o are constants to be determined. Glass transition and glass softening are obtained from dilatometer (Table 2). Beamann equation i.e. $T_g/T_m = 2/3$ is used to determine the melting temperature [53]. For the viscosity/temperature curve for silicate melts, a number of specific viscosities has been designated as the reference points corresponding to different temperatures. The viscosity value at T_g, T_d and T_m are reported to be $10^{13.6}$, $10^{11.3}$ and 10^6 dPaS respectively. A, B and T_o are determined from three equations by substituting these viscosity values corresponding to T_g, T_d and T_s. By solving the coupled equations, viscosity is obtained. The values of viscosity for all composites at 800 °C are listed in Table 2. The variation of viscosity with temperature for all the composites is shown in Fig. 3. The viscosity follows the order

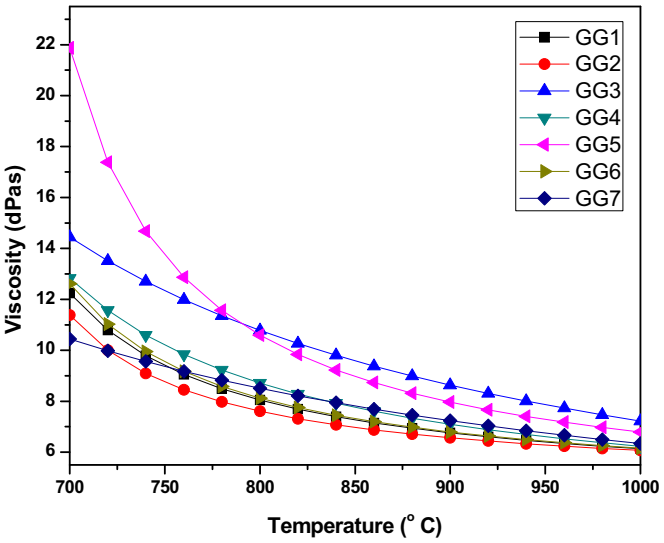

Fig. 3. Variation of viscosity with temperature for all composites.

Table 2
CTE, characteristic temperatures, viscosity, activation energy, weight loss and frequency factor for all glass composites.

Sample	CTE (RT-softening) $\times 10^{-6}$ K^{-1}	CTE after 1000 h (RT-softening) $\times 10^{-6}$ K^{-1}	T_g (DIL in °C)	T_s (DIL in °C)	T_g (DTA in °C)	T_c (DTA in °C)	Viscosity η (dPaS)	Activation energy (kJ mol^{-1})	Frequency factor (ν)	Weight loss (%)
GG1	8.31	9.36	687	712	694	828	8.05	273	2.32×10^{12}	3.64
GG2	8.43	9.92	681	701	686	843	7.61	356	8.67×10^{8}	1.83
GG3	8.21	10.89	730	775	741	867	9.05	295	2.16×10^{11}	1.31
GG4	8.50	9.32	692	727	701	834	8.71	282	1.74×10^{12}	2.89
GG5	8.52	7.05	751	785	759	848	10.59	289	4.57×10^{12}	1.92
GG6	8.74	10.01	691	716	693	861	8.12	304	3.51×10^{10}	0.58
GG7	8.19	9.77	698	774	704	856	8.51	299	6.44×10^{11}	0.93

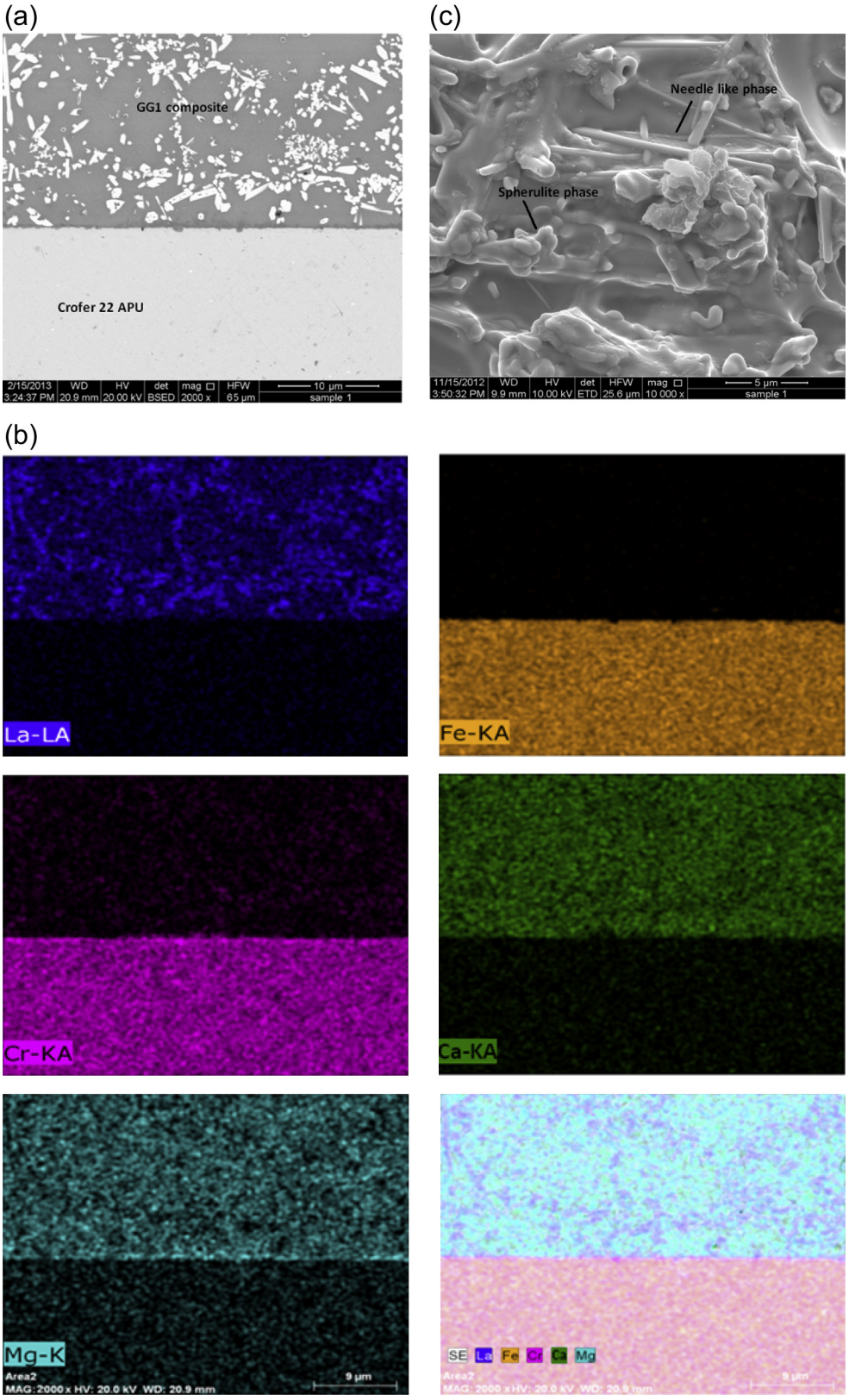

Fig. 4. (a) Crofer 22APU/GG1 diffusion couple (b) X-ray dot mapping of Crofer 22APU/GG1 couple and (c) microstructure of GG1 composite after heat-treatment at 850 °C for 1000 h.

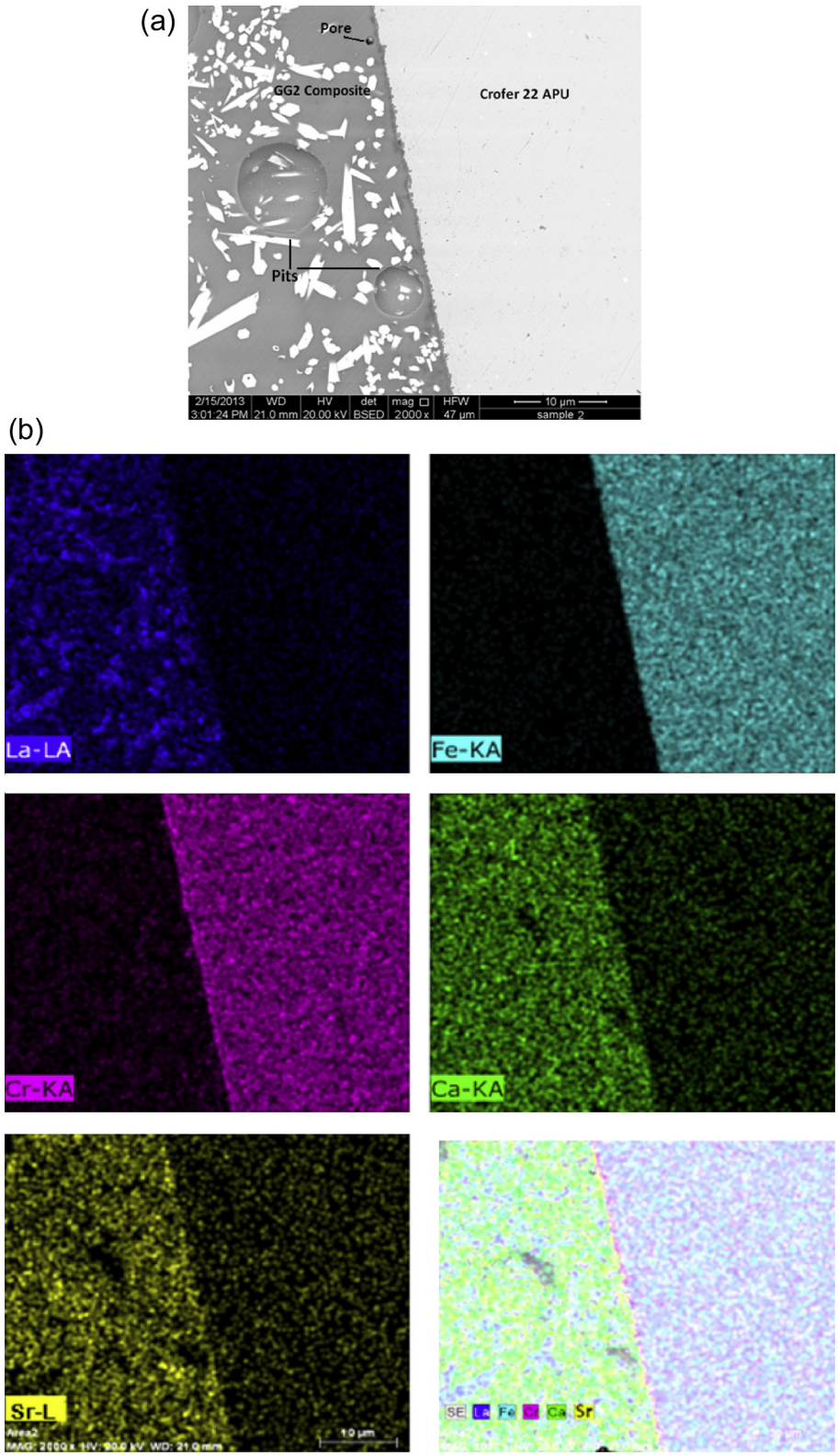

Fig. 5. (a) Crofer 22APU/GG2 diffusion couple and (b) X-ray dot mapping of Crofer 22APU/GG2 couple after heat-treatment at 850 °C for 1000 h.

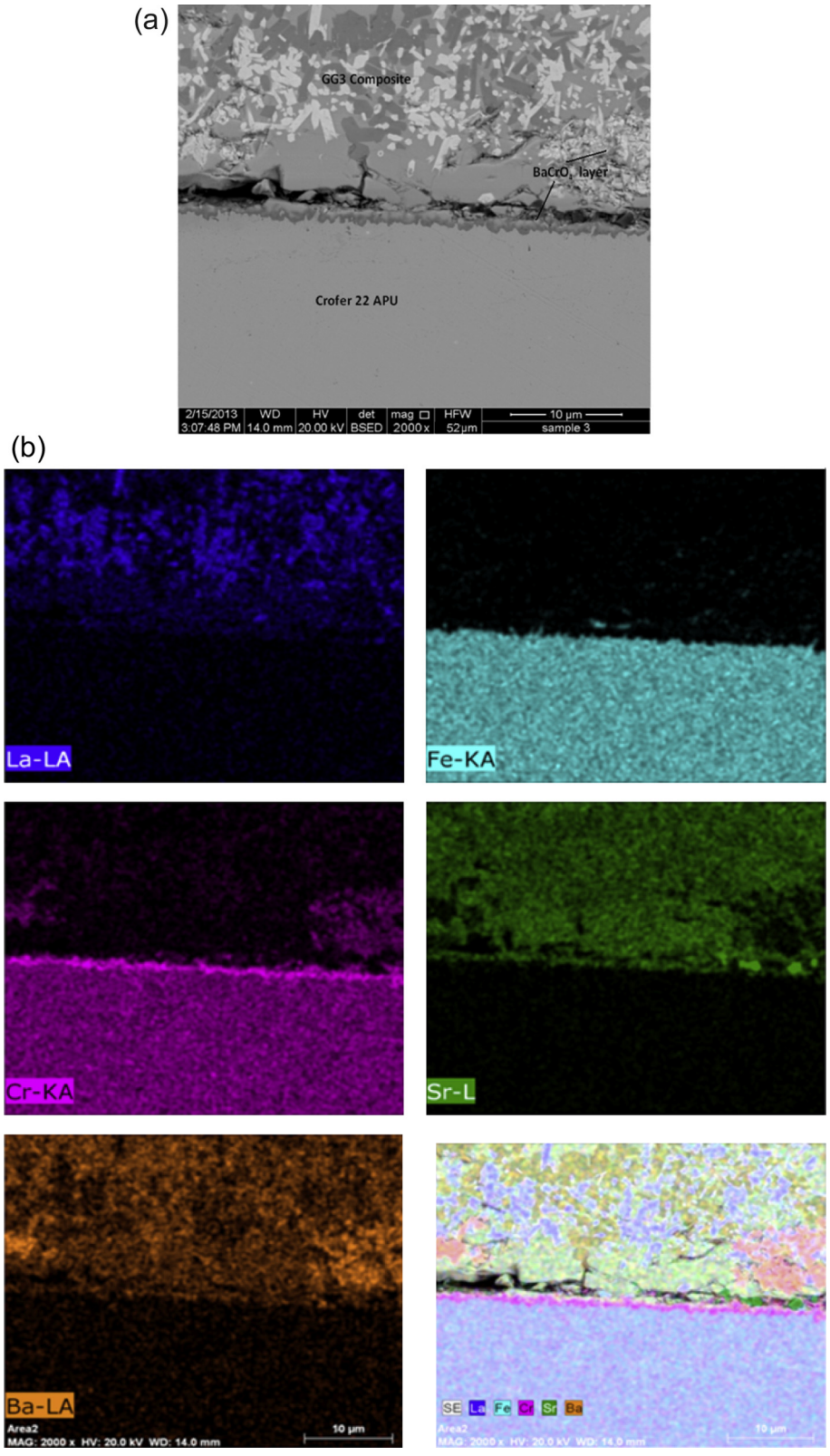

Fig. 6. (a) Crofer 22APU/GG3 diffusion couple and (b) X-ray dot mapping of Crofer 22APU/GG3 couple after heat-treatment at 850 °C for 1000 h.

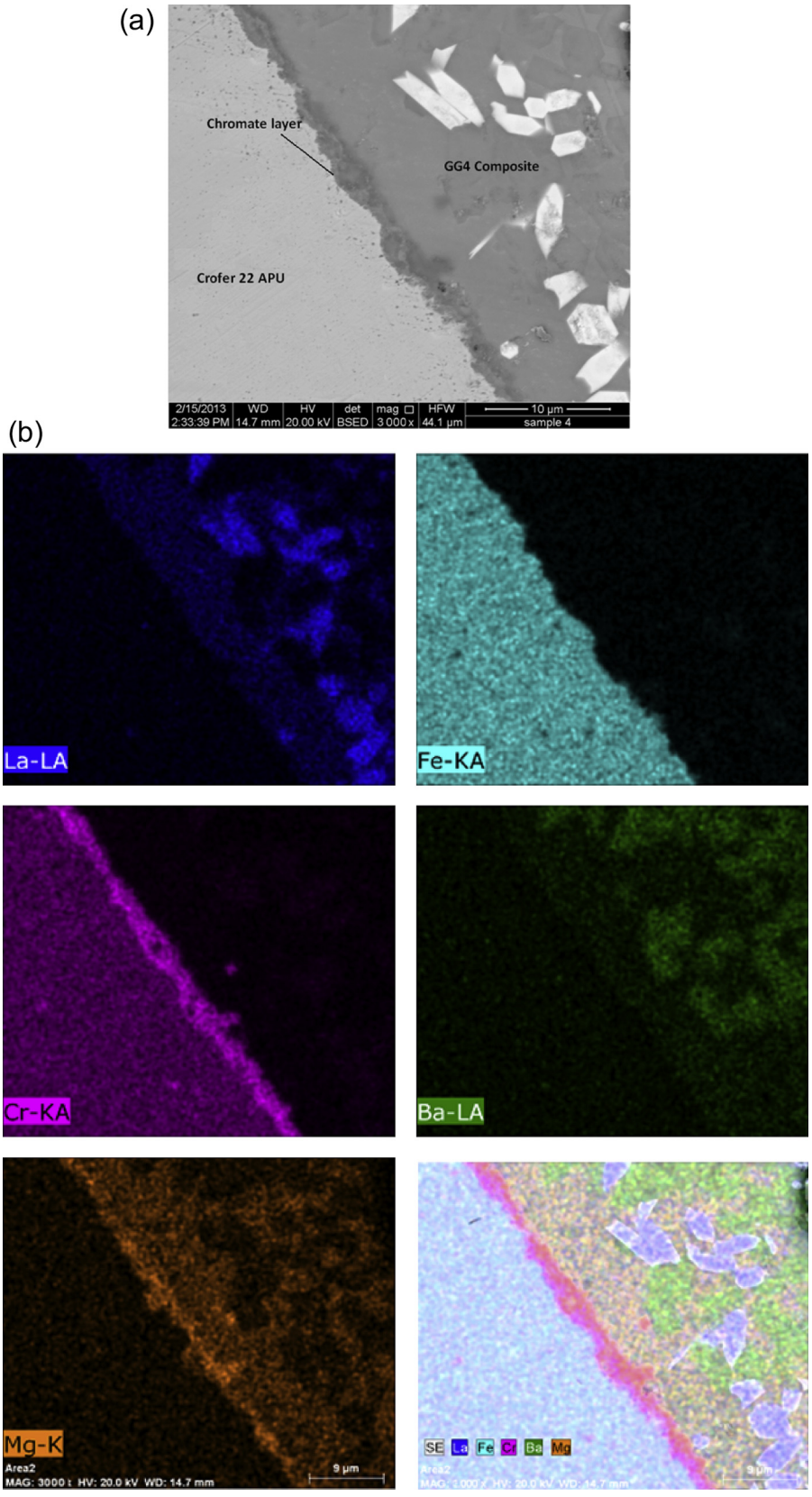

Fig. 7. (a) Crofer 22APU/GG4 diffusion couple and (b) X-ray dot mapping of Crofer 22APU/GG4 couple after heat-treatment at 850 °C for 1000 h.

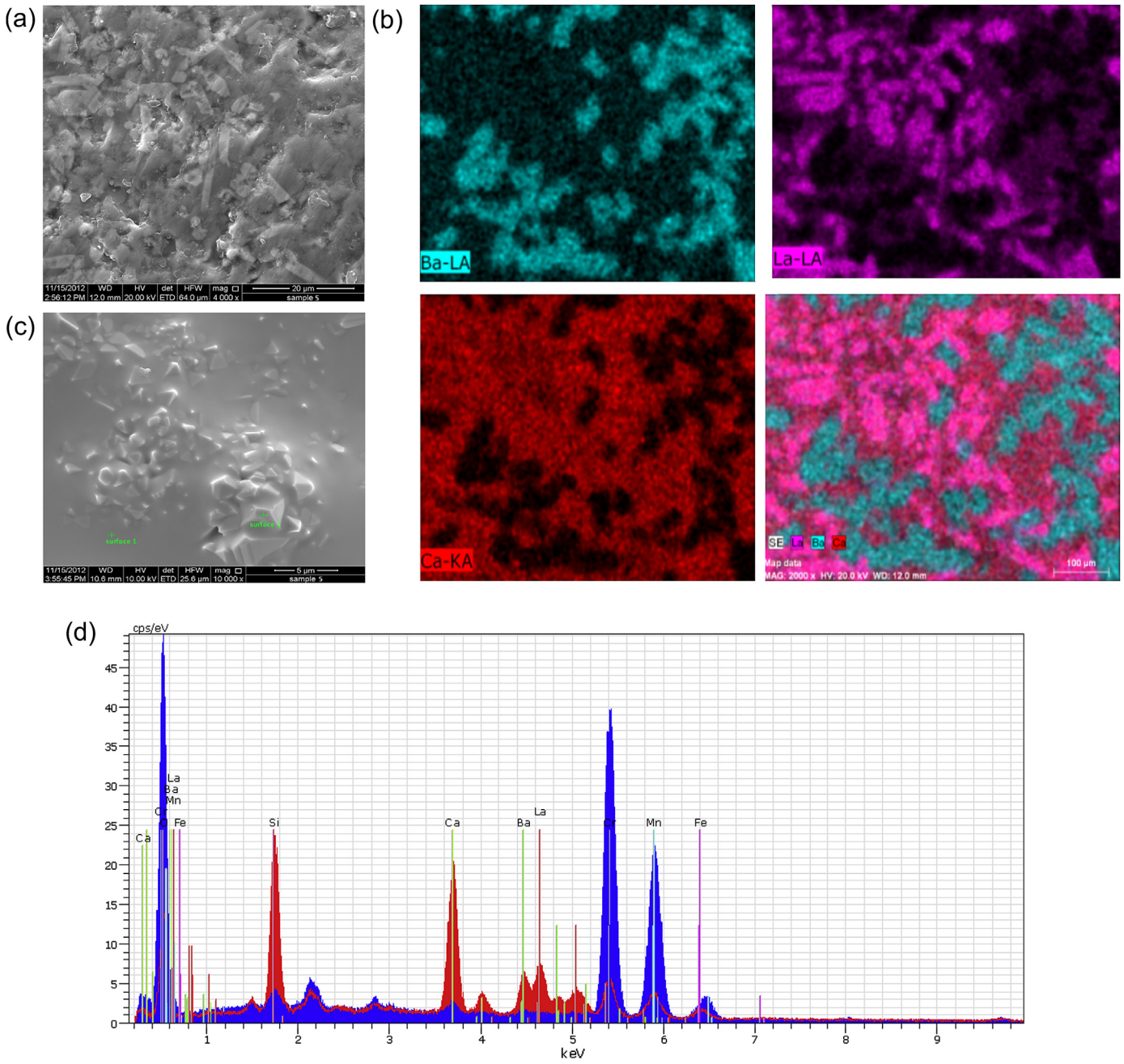

Fig. 8. (a) Microstructure of delaminated GG5 composite (b) X-ray dot mapping of delaminated GG5 composite (c) microstructure of delaminated Crofer 22APU and (d) multipoint EDS analysis on the surface of delaminated Crofer 22APU after heat-treatment at 850 °C for 1000 h.

GG5 > GG3 > GG4 > GG7 > GG6 > GG1 > GG2 and decreases with increasing temperatures. For sealing applications, the required viscosity criterion is 10^6–10^9 dPaS [45,46,54]. All the glasses except GG5 satisfy this criterion.

Table 3
Composition analysis by EDS for sample GG5 (elements in mass %).

Spectrum	O	Si	Ca	Cr	Mn	Fe	Ba	La
GG 5 surface 1	28.65	11.19	15.66	4.97	4.78	2.35	13.67	18.73
GG 5 surface 2	33.55	0.55	0.81	39.60	21.63	2.07	0.80	0.99
Mean value	31.10	5.87	8.23	22.29	13.21	2.21	7.23	9.86
Sigma	3.46	7.52	10.50	24.49	11.92	0.19	9.10	12.55
Sigma mean	2.45	5.32	7.43	17.32	8.43	0.14	6.43	8.87

3.5. Sealing and microstructural analysis

It is necessary to monitor the interfacial chemical reactions thoroughly to gain an insight of composite/interconnect interaction. Generally diffusion occurs prior to chemical reaction. Sometimes chemical reactions are detrimental in nature leading to microstructural modifications, hence hindering the functioning of SOFC. In the present section, the diffusion couple of the glass composites with Crofer 22APU heat-treated at 850 °C for 1000 h have been investigated in order to check the interfacial stability and chromate formation. Chromium diffusion follows a two-step process i.e. during first stage at 800 °C, chromium comes out of Crofer 22APU alloy and reacts with non-bridging oxygens (NBO) to form

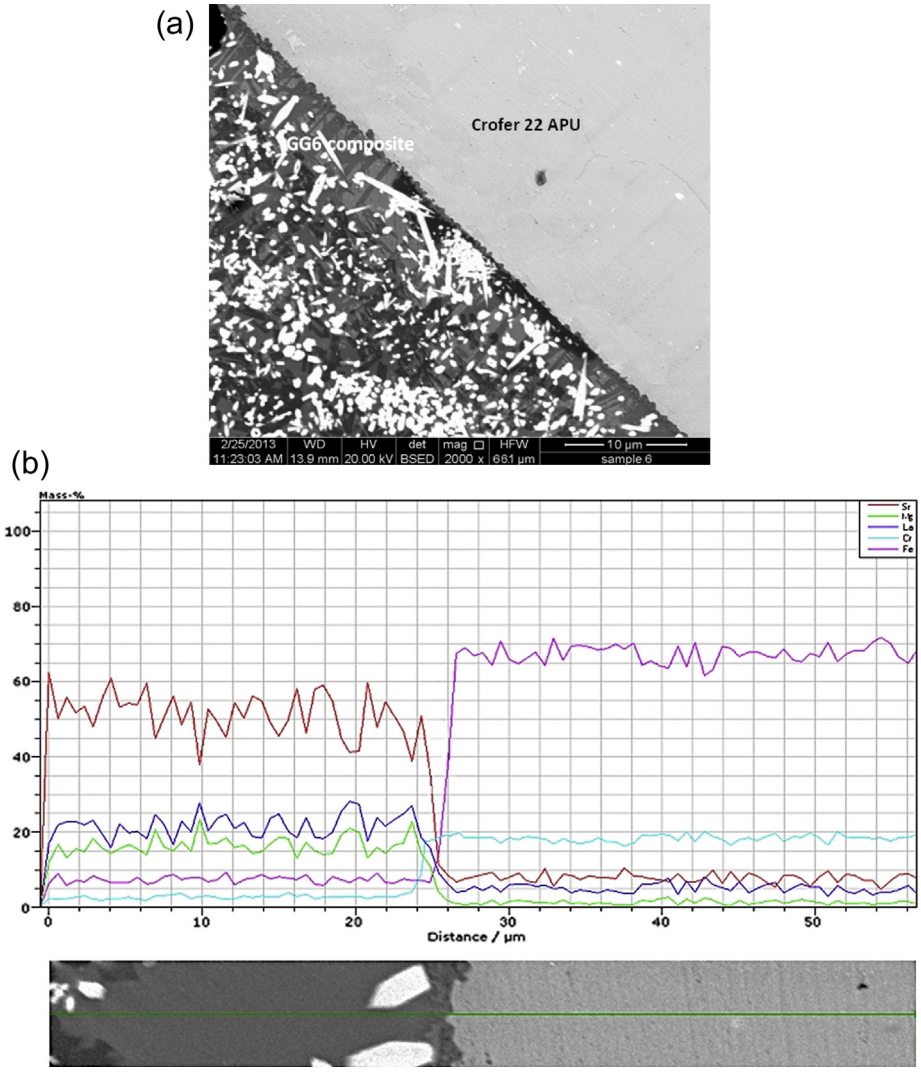

Fig. 9. (a) Crofer 22APU/GG6 diffusion couple and (b) EPMA analysis of Crofer 22APU/GG6 couple after heat-treatment at 850 °C for 1000 h.

Cr_2O_3. During the second stage, Cr_2O_3 can condense and form Cr_2O_3 films [55] at the interface. Sometimes the chromia layer reacts with the seal glass to form undesirable chromate products. Diffusion of Crofer 22APU elements into glass breaks the glass network structure, which further enhances devitrification of glass [32].

From Fig. 4(a), it is clear that GG1 glass has revealed good adhesion with Crofer 22APU interconnect even after prolonged duration of heat-treatment for 1000 h. Some closed pits could be seen on the glass side, which could have been due to the internal residual stresses within the amorphous glass. Usually the closed pits are considered to be non-problematic as they are impermeable to gas flow [56]. Furthermore, elemental analysis from dot-mapping (Fig. 4(b)) has indicated no diffusion of lanthanum and iron on either side of interface. Magnesium and calcium has diffused out of the glass toward the interconnect. Ca^{2+} and Mg^{2+} have small ionic radii, hence their diffusion kinetics are fast. The interface is free of any corrosion reaction products. Fig. 4(c) shows the microstructure of GG1 glass after 1000 h treatment at 850 °C. The microstructure shows needle shape phases and spherulite phase along with residual amorphous glassy matrix. This is in complete agreement with the XRD results as $CaMgSi_2O_6$ and $La_{9.33}Si_6O_{26}$ phases have been reported during the present investigation. Hence the composite exhibited controlled crystallization, which is a favorable microstructure. Examination around the seal region of GG2 composite/Crofer 22APU has revealed very good adhesion as is clear from Fig. 5(a). The interface is continuous and devoid of cracks. The interior of the composite has some closed pits and pores, which could be attributed to thermal stresses generated within the glass or volatility of entrapped gases. Sometimes the alloy element diffuses into the glass region. They react with glass components or impurities present leading to formation of gaseous phases. These gases remain entrapped in glass and subsequently lead to pore formation. Generally the gas phase is hydrogen and formed via following reaction [57]:

$$xM_{(alloy)} + yH_2O \rightarrow M_xO_y + yH_2 \quad (3)$$

When M is chromium, then the Gibbs free energy of reaction is very small i.e. −222 kJ mol^{-1}. For M to be iron, the Gibbs free energy is −55 kJ mol^{-1}. Hence, the reactions with chromia are most energetically favored one. During the prolonged heat-treatment of the glass composite, crystallization takes place leading to phase formation. These phases may force the pores to migrate into the sealing glass. The amorphous content of the GG2 glass composite is higher as

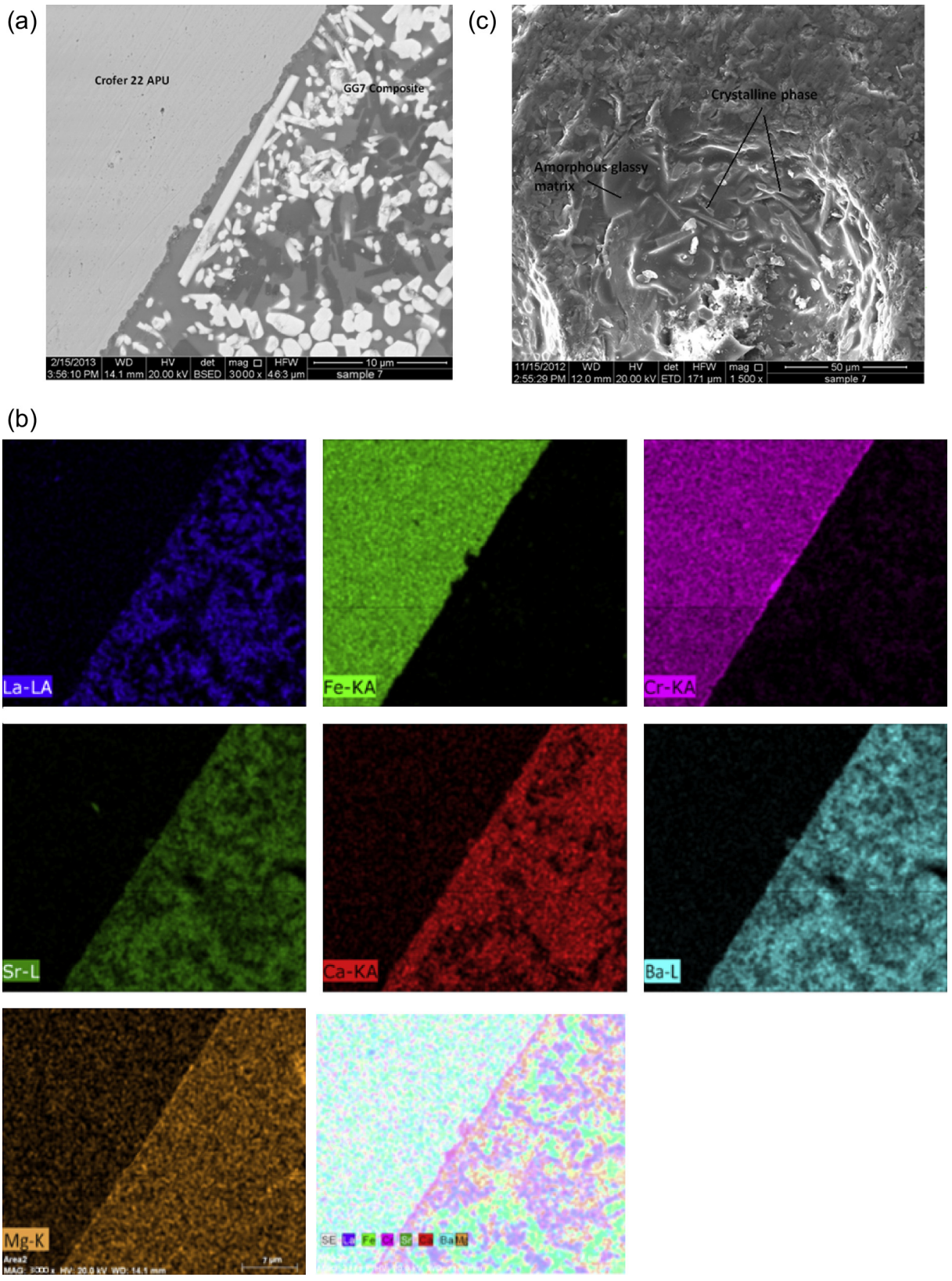

Fig. 10. (a) Crofer 22APU/GG7 diffusion couple (b) X-ray dot mapping of Crofer 22APU/GG7 couple and (c) microstructure of GG7 composite after heat-treatment at 850 °C for 1000 h.

is clear from XRD analysis (Fig. 2). The high activation energy of crystallization of GG2 among all other composites prevents its devitrification. This high amorphous content in the glass composite even after heat-treatment of 1000 h may contribute to internal brittleness, eventually leading to pit formation. From the dot mapping of the GG2 composite (Fig. 5(b)), it is clear that iron has not diffused out of the alloy. Ca^{2+}, La^{3+} and Sr^{2+} have diffused considerably out of glass matrix. Diffusion of the chromium ion has taken place without any accumulation or segregation at the interface.

For the GG3 composite/Crofer 22APU diffusion couple, there is delamination along the interface as indicated from Fig. 6(a). Dot-mapping of the GG3 composite (Fig. 6(b)) clearly reveals the formation of $BaCrO_4$ phase and chromia layer at interface. Chromium has diffused toward the glass composite side and reacted with Ba^{2+} ions in the glass network. $BaCrO_4$ is an orthorhombic compound having high CTE and is mainly formed at the edge or near the edge areas where oxygen is easily accessible [58]. The region near $BaCrO_4$ formation has shown crack formation. The $BaCrO_4$ formation might have the following reaction kinetics [59]:

$$2Cr_2O_3 + BaO + 3O_2 \rightarrow 4BaCrO_4 \quad (4)$$

When chromium oxyhydroxide reacts with BaO, then $BaCrO_4$ is formed but it causes subsequent porosity in the glass network due to formation of the water vapors. But as no porosity is apparent in the glass network, hence the reaction kinetics must have probably taken place due to interaction between the chromia scale and the sealing glass composite [59]. But the formation of $SrCrO_4$ is completely precluded in sample GG3. Hence there is competition between Ba^{2+} and Sr^{2+} ions to form chromate, but barium possesses higher affinity for chromate formation. Iron has not diffused on either side of the interface, though lanthanum has diffused out of the glass matrix. The chemical interaction between GG3 and the interconnect lead to gaps at the edges of the joint region. In case of GG4 composite/Crofer 22APU diffusion couple, the interface has shown no pores or cracks and has shown good adhesion as indicated by Fig. 7(a). Good interconnect alloy/glass composite bond is observed at the interface. The X-ray dot mapping (Fig. 7(b)) shows the migration of Mg^{2+} ions toward the interface. Diffusion of magnesium has been highest among all other cations on account of its small atomic size. Non-uniform chromium accumulation has also been observed at the joint sealing region. This indicates the possible formation of $MgCrO_4$ at the interface. No segregation of barium is seen though it has diffused on either side of the interface, precluding the possibility of barium chromate formation. Iron has not diffused out whereas diffusion of lanthanum is considerable.

For GG5 composite/Crofer 22APU couple, the interface gets delaminated after heat-treatment. This could be due to the formation of the $CaSiO_3$ phase in the glass composite after 1000 h heat-treatment. Calcium silicate is a low CTE phase. The CTE of the glass composite has also decreased from 8.52×10^{-6} K^{-1} to 7.05×10^{-6} K^{-1}. In addition to this, the high viscosity obtained for this composite also decreases its wetting characteristics. Fig. 8(a) shows the microstructure at the interface area of the detached glass composite. The elemental analysis of Ba, Ca and Si is shown in Fig. 8(b). This clearly indicates phase formation embedded in amorphous glassy matrix, which is in correlation with the XRD analysis. Fig. 8(c) shows the microstructure near the interfacial sealing region of Crofer 22APU. Some crystals could be seen at the surface. The comparative multipoint elemental composition on the crystal surface and the Crofer surface is given in Table 3. Diffusion of calcium, barium and lanthanum could be seen on either side of interface. Fig. 8(d) presents the multipoint energy dispersive spectroscopy (EDS) clearly indicating the presence of chromium, manganese, iron and oxygen suggesting the formation of (Cr, $Mn)_3O_4$ spinel phase. Surprisingly, the spinel is considered to be a stable metal oxide coating [27]. Generally, this layer acts as a transition layer to promote strong chemical bonding at the interface. The spinel layer prevents the formation of chromate and corrosion at the interface, hence the delamination is not possible due to chromate formation. But the $CaSiO_3$ phase formation and high viscosity of GG5 composite might have lead to its detachment at the interface. High viscosity of the composite also reduces its wettability with adjoining components.

In the GG6 glass composite, no delamination or reaction zone could be seen at the interface as revealed by Fig. 9(a). At both edge and interior region, the composite is well bonded to the interconnect. The interfacial region as well as the glass microstructure is more or less defect free for this composition even when viewed after prolonged heat-treatment of 1000 h at 850 °C. Electron probe microanalysis (EPMA) for elemental variation around the seal region is shown in Fig. 9(b). EPMA indicates the absence of reaction products at the interface. Iron and chromium diffusion follow 'S' type profile whereas magnesium, strontium and lanthanum follow 'Z' type profile [33–36]. The profiles of Mg, Sr and La have oscillations attributed to compositional difference between devitrified and glassy phase or interaction between X-rays of different elements [60]. The spikes are almost absent in Fe and Cr profile indicating their homogenous distribution. Surprisingly, the chromium diffusion toward the glass side is relatively less than the iron diffusion. The diffusion of ions also leads to strong mechanical interlocking [27]. Diffusion of strontium is highest followed by lanthanum and magnesium diffusion. GG7 glass composite also exhibits very good bonding characteristics without the formation of any detrimental reaction products or delamination at the joint region (Fig. 10(a)). No corrosion is seen around the sealing region, which is further supported by dot-mapping shown in Fig. 10(b). No formation of chromates is apparent, though subsequent diffusion of calcium and magnesium ions has been observed. Strontium, lanthanum and barium have depicted sluggish diffusion kinetics on account of their bigger atomic size. Fig. 10(c) is the microstructure of GG7 glass after 1000 h treatment at 850 °C, which is clearly depicting the needle like crystalline phases embedded inside the amorphous matrix. But as is clear from XRD analysis, almost all the composites have controlled crystallization, which is very favorable for sealing applications.

4. Conclusions

The particle size and zeta potential for the GG1 composite is smallest which could be due to small ionic size of magnesium and calcium. The activation energy of crystallization is lowest for the GG1 composite whereas the GG2 composite exhibits the highest activation energy of glass crystallization. All the seven glass composites have shown phase formation after 1000 h heat-treatment at 850 °C. Only the GG2 composite is single phase whereas all other composites have shown double phase formation. All glass composites exhibited acceptable CTE except GG5. The GG5 composite has shown the formation of very low CTE calcium silicate which may be responsible for its delamination from interconnect Crofer 22APU. Moreover, the viscosity of GG5 is highest which further resists its wetting capability. This has consequently lead to delamination of the GG5 composite from Crofer 22APU interconnect in spite of the formation of stable spinel oxide layer on Crofer 22APU surface. GG3 and GG4 composites have shown chromate formation, though no delamination has been observed at the interface of GG4 with Crofer 22APU. GG1 composite also have some porosity due to internal residual stress. At the same time, closed pits are observed in the GG2 composite. Good bonding behavior has been demonstrated by the GG6 and the GG7 composite. The hermeticity and gas tightedness of these composites along with low

embrittlement indicate that these composites may work as sealants in real SOFC conditions.

Acknowledgment

The authors are thankful to CIES, Washington D.C. for financial support and Mr. Steve McCartney, NCFL/ICTAS, Virginia Tech for his help and cooperation during electron microscopy. One of the authors (GK) is thankful to Dr. Vishal Kumar and Mr. Adam Floyd, Virginia Tech for their consistent guidance.

References

[1] S.C. Singhal, K. Kendall, High Temperature Solid-oxide Fuel Cells: Fundamentals, Elsevier, New York, 2000, p. 14.
[2] B.C.H. Steele, A. Heinzel, Nature 414 (2001) 345–352.
[3] N.Q. Minh, Solid State Ionics 174 (2004) 271–277.
[4] S.M. Haile, Acta Mater. 51 (2003) 5981–6000.
[5] J.W. Donald, P.M. Mallinson, B.L. Metcalfe, L.A. Gerrard, J.A. Fernie, J. Mater. Sci. 46 (2011) 1975–2000.
[6] J.M. Ralph, A.C. Schoelar, M. Krumpelt, J. Mater. Sci. 36 (2001) 1161–1172.
[7] K.A. Nielsen, M. Solvang, S.B.L. Nielsen, A.R. Dinesen, D. Beeaff, P.H. Larsen, J. Eur. Ceram. Soc. 27 (2007) 1817–1822.
[8] Y.S. Chou, J.W. Stevenson, J. Mater. Res. 18 (2003) 2243–2250.
[9] K. Kendall, Int. J. Appl. Ceram. Technol. 7 (2010) 1–9.
[10] S.P.S. Badwal, Solid State Ionics 143 (2001) 39–46.
[11] F. Smeacetto, M. Salvo, M. Ferraris, J. Cho, A.R. Boccaccini, J. Eur. Ceram. Soc. 28 (2008) 61–68.
[12] M.K. Mahapatra, K. Lu, Mater. Sci. Eng. R 67 (2010) 65–85.
[13] J.W. Fergus, J. Power Sources 147 (2005) 46–57.
[14] K.S. Weil, C.A. Coyle, J.S. Hardy, J.Y. Kim, G.G. Xia, Fuel Cells Bull. (May 2004) 12–16.
[15] K.S. Weil, J. Miner. Met. Mater. Soc. 58 (2006) 37.
[16] S. Le, K. Sun, N. Zhang, Y. Shao, M. An, Q. Fu, X. Zhu, J. Power Sources 168 (2007) 447–452.
[17] V. Kumar, Rupali, O.P. Pandey, K. Singh, Int. J. Hydrogen Energy 36 (2011) 14971–14976.
[18] P.H. Larsen, P.F. James, J. Mater. Sci. 33 (1998) 2499–2507.
[19] N. Lahl, D. Bahadur, K. Singh, L. Singheiser, K. Hilpert, J. Electrochem. Soc. 149 (2004) A607.
[20] M.K. Mahapatra, K. Lu, W.T. Reynolds, J. Power Sources 179 (2008) 106–112.
[21] Y.S. Chou, J.W. Stevenson, G.G. Xia, Z.G. Yang, J. Power Sources 195 (2010) 5666–5673.
[22] M.J. Pascual, A. Guillet, A. Duran, J. Power Sources 169 (2007) 40–46.
[23] S.M. Gross, T. Koppitz, J. Remmel, J.B. Bouche, U. Reisgen, Fuel Cells Bull. (September 2006) 11–15.
[24] X. Deng, J. Duquette, A. Petric, Int. J. Appl. Ceram. Technol. 4 (2007) 145–151.
[25] F. Smeacetto, M. Salvo, M. Ferraris, V. Casalegno, P. Asinari, J. Eur. Ceram. Soc. 28 (2008) 611–616.
[26] N.P. Bansal, E.A. Gamble, J. Power Sources 147 (2005) 107–115.
[27] K.A. Nielsen, M. Solvang, F.W. Poulsen, P.H. Larsen, Evaluation of Sodium Aluminosilicate Glass Composite Seal with Magnesia Filler, in: 28th IDACC: Ceramics Engineering and Science Proceedings, vol. 25, John Wiley and Sons, Hoboken, NJ, USA, 3 June 2008.
[28] S.B. Sohn, Se-Y. Choi, J. Am. Ceram. Soc. 87 (2004) 254–260.
[29] M. Brochu, B.D. Gauntt, R. Shah, G. Miyake, R.E. Loehman, J. Eur. Ceram. Soc. 26 (2006) 3307–3313.
[30] R. Loehman, H.P. Dumm, H. Hofer, Proc. Ceram. Eng. Sci. 23 (2002) 699–710.
[31] G. Kaur, O.P. Pandey, K. Singh, Int. J. Hydrogen Energy 37 (2012) 3883–3889.
[32] G. Kaur, O.P. Pandey, K. Singh, Int. J. Hydrogen Energy 37 (2012) 6862–6874.
[33] G. Kaur, O.P. Pandey, K. Singh, Int. J. Hydrogen Energy 37 (2012) 17235–17244.
[34] G. Kaur, O.P. Pandey, K. Singh, J. Electrochem. Soc. 159 (2012) F717–F724.
[35] G. Kaur, O.P. Pandey, K. Singh, Fuel Cells 12 (2012) 739–748.
[36] G. Kaur, O.P. Pandey, K. Singh, Int. J. Appl. Ceram. Technol., http://dx.doi.org/10.1111/ijac.12002.
[37] W.J. Wnek, J. Colloid Interface Sci. 60 (1977) 361–375.
[38] K. Makino, T. Yamada, M. Kimura, T. Oka, H. Ohshima, T. Kondo, Biophys. Chem. 41 (1991) 175–183.
[39] S.K. Lee, B.O. Mysen, G.O. Cody, Phys. Rev. B 68 (2003) 214206–214213.
[40] A.J.G. Ellison, P.C. Hess, J. Non-Cryst. Solids 127 (1991) 247.
[41] C.I. Merzbacher, B.L. Sheriff, J.S. Hartman, W.B. White, J. Non-Cryst. Solids 124 (1990) 194.
[42] V. Raghvan, Materials Science and Engineering, fifth ed., 2008.
[43] J.A. Augis, J.E. Bennett, J. Therm. Anal. Calor. 13 (1978) 283–292.
[44] G.O. Piloyan, J.D. Rybachikov, O.S. Novikova, Nature 212 (1996) 1229.
[45] V. Kumar, G. Kaur, O.P. Pandey, K. Singh, Phys. Chem. Glasses 52 (2011) 212–220.
[46] V. Kumar, O.P. Pandey, K. Singh, Phys. B 405 (2010) 204–207.
[47] T. Jin, K. Lu, J. Power Sources 195 (2010) 195–203.
[48] J.E. Shelby, Introduction to Glass Science and Technology, second ed., The Royal Society of Chemistry, Cambridge, 2005.
[49] W.D. Kingery, H.K. Bowen, D.R. Uhlmann, Introduction to Ceramics, second ed., John Wiley and Sons, New York, 1976.
[50] W. Liu, X. Sun, M. Khaleel, J. Power Sources 185 (2008) 1193–1200.
[51] M.C. Wilding, A. Navrotsky, J. Non-Cryst. Solids 265 (2000) 238–251.
[52] A. Goel, M.J. Pascaul, J.M.F. Ferreira, Int. J. Hydrogen Energy 35 (2010) 6911–6923.
[53] R.G. Beaman, J. Polym. Sci. 21 (1956) 223–235.
[54] S. Ghosh, P. Kundu, A. Das Sharma, R.N. Basu, H.S. Maiti, J. Eur. Ceram. Soc. 28 (2008) 69–76.
[55] E. Konysheva, V. Seelnig, A. Bemsehn, L. Singheiser, K. Hilpert, J. Mater. Sci. 42 (2007) 5778–5784.
[56] A. Karamanov, L. Arrizza, I. Matekovits, M. Pelino, Ceram. Int. 30 (2004) 2129–2135.
[57] Z. Yang, G. Xia, K. Scott Well, J.W. Stevenson, K.D. Meinhardt, J. Mater. Eng. Perform. 13 (2004) 327–334.
[58] Z. Yang, J.W. Stevenson, K.D. Meinhardt, Solid State Ionics 160 (2003) 213–225.
[59] Z. Yang, K.D. Meinhardt, J.W. Stevenson, J. Electrochem. Soc. 150 (2003) A1095–A1101.
[60] M.K. Mahapatra, K. Lu, J. Power Sources 196 (2011) 70.